Flow-field fitting method and acoustic Doppler velocity measurement: a new approach and its application to the detection of leakage pathways in the concrete face rockfill dam

Xiang Zhao[1], **Hongbing Zhang**[1,*], **Kuiye Wei**[1,2] , **Ping Wang**[1], **Quan Ren**[1], **Dailu Zhang**[1]

1.College of Earth Science and Engineering, Hohai University, Nanjing, 211100, China

2. Anhui and Huaihe River Water Resources Institute, Bengbu, 233000, China

* Corresponding author: hbzhang@hhu.edu.cn (Hongbing Zhang)

zhaoxiang1109@hhu.edu.cn (Xiang Zhao), weikuiye@126.com (Kuiye Wei), pingwang@hhu.edu.cn (Ping Wang), renquanlogo@163.com (Quan Ren), 181309080004@hhu.edu.cn (Dailu Zhang)

Key points:

1.The methods we proposed are first used to detect the location of the leakage inlets and leakage pathways in the concrete face rockfill dam.

2. Numerical simulation show the seepage field can be fitted with current field, and leakage can be effectively detected in the current field.

3. The combination of two methods formed a novel leakage and pathways detection method in the concrete face rockfill dam.

Abstract

The paper is to detect the leakage inlets, determine the leakage pathways through the dam, and ensure that the amount of the leakage in the upstream and downstream is consistent, and that there is no leakage around the concrete face rockfill dam. The injection of a pseudo-random current in the water between two aluminum sheets A and B generates a current field that can be measured in the water with sensitive current sensors. When the current is channeled along leakage pathways, the flow-field fitting method can be used to detect these inlets of the leakage pathways. We first review the background equations for the seepage field and the current field in the flow-field fitting method, and we also use an approach to calculate the discharge and ensure the consistency of the upstream and downstream leakage based on the Doppler effect in physics. Moreover, to illustrate how the flow-field fitting method works, we use numerical simulation method to verify the feasibility of the flow-field fitting method. Lastly, we proceed with a case study for which the flow-field fitting method and the acoustic Doppler flow velocity measurement are used to identify and map potential leakage pathways bypassing upstream into the flow measurement weir of the downstream. The approaches proposed in this paper successfully detect three leakage areas and obtain the discharge. The results of detected in a case study provide engineering geology information for optimizing the layout of grouting holes.

Keywords: Concrete face rockfill dam, Leakage pathways, flow-field fitting method, Doppler effect, Numerical simulation

Plain Language Summary

The approaches proposed in this paper are first used to detect leakage inlets and the leakage pathways in the concrete face rockfill dam. We use numerical simulation to verify the feasibility of the flow-field fitting method, and based on the Doppler effect in physics, we ensure that the amount of the leakage in the upstream and downstream is consistent, and that there is no leakage around the concrete face rockfill dam. We use the approaches we proposed successfully detect three leakage areas and obtain the discharge in the concrete face rockfill dam. The results of detected in a case study provide engineering geology information for optimizing the layout of grouting holes. The methods and results can be used as a reference for other similar engineering leakage problems.

1.Introduction

A concrete face rockfill dam (CFRD) is a type of dam that is widely used in water conservancy and hydropower projects around the world. The concrete slab supported and stabilized by the rockfill material below is connected to the toe slab through peripheral joints to form an impervious system. The leakage through a dam can lead to water loss, and serious leakage can reduce the project benefits and even dam failure (e.g., Gutierrez et al., 2003; Howard and McLane Iii, 1988; Ferdos et al., 2018). Therefore, we need to conduct leakage detection on the dam after the dam is built or a regular basis. Geophysical techniques are often used to detect the anomalous areas and leakage pathways. The geophysical methods used depend on the type of problem to be studied. Generally, mainly include: self-potential (SP) method, Ground Penetrating Radar (GPR) method, induced polarization (IP) method, electrical resistivity imaging (ERI) and so on.

The SP method (e.g., Rizzo et al., 2004; Jardani et al., 2006a; Jardani et al., 2008; Ahmed et al., 2020) is a suitable method for large scale investigation of earth dams, and it can localize seeps and determine permeability. However, for complex dam, SP method is difficult to quantify, and it is difficult to distinguish whether SP anomaly is the response of the leakage site, which may lead to misjudgment. The GPR method (e.g., Xu et al., 2010; Prinzio et al., 2012; Antoine et al., 2015) can identify internal erosion of dams' inner structure. However, GPR method has a shallow depth of detection, and this limitation limits the application of this method in dams. The IP method (e.g., Revil et al. 2015; Martínez-Moreno et al., 2018; Abdulsamad et al., 2019) can be used to estimate water content or saturation values effectively, and it is sensitive to permeability but suffer from limitations regarding its resolution. The ERI method is valuable for imaging the foundations of earth dams and delineating leakage zones, but it is limited by its lack of resolution (e.g., Cho and Yeom,2007; Dahlin, T et al., 2008; Bolève et al., 2012; Revil, A et al.,2012). Other methods, temperature field detection method and fluorescent tracer tests (e.g., Unal et al., 2007; Fargier et al., 2014; Battaglia et al., 2016), which are only used as an auxiliary method in leakage detection, and are usually used in combination with the other geophysical methods to identify the position of leakages. However, for CFRD, the GPR and ERI method are not

applicable, because the surface of the CFRD is concrete. In addition, the reservoir area has strong winds and waves, the SP method is also not suitable.

In order to detect the leakage inlets, determine the leakage pathways through the dam, and ensure that the amount of the leakage in the upstream and downstream is consistent, the flow-field fitting method and acoustic Doppler velocity measurement are proposed. The flow-field fitting method is a means to detect the leakage distribution characteristics by fitting the seepage field with the current field. In hydraulics, the seepage field will be generated around the leakage inlets in dams. It is hardly to detect directly fluctuations generated by the seepage field with the existing techniques, so the existence of such weak seepage field can only be measured indirectly. He et al. (1999) used the flow-field fitting method to detect the piping of embankment during the flood season and successfully locate the leakage location. Qianwei et al. (2017) and Meng et al. (2018) used the flow-field fitting method to determine the location of the leakage inlets in the concrete dam's upstream face. Moore et al. (2011), Meng et al. (2018) and Ahmed et al. (2019) numerically simulated leakage pathways based on current field in the structure of the dam, and it showed that leakage inlets can be detected in the upstream face successfully. We did a numerical simulation of the CFRD based on the seepage field and the current field, it showed that the flow-field fitting method can be used to effectively detect the leakage inlets in the CFRD of the study area. We inject the pseudo-random current between two aluminum sheets A and B in the water which generates a current field that can be measured with sensitive current sensors.

The acoustic Doppler velocity measurement uses acoustic signals and the Doppler shift to analyze flow velocity. Flow velocity is obtained by measuring Doppler pulse shifts back-scattered by particles located in water cells allocated along the instrument's measurement range (Marc et al., 2020). This technology has been extensively used for flow velocity and discharge analysis in natural rivers and streams (e.g., Gunawan et al., 2010; Boldt and Oberg, 2015), oceans (Münchow et al., 1995) and man-made channels (e.g., Oberg et al., 2007; Bahreinimotlagh et al. 2016; Klema et al. 2020). It showed that the acoustic Doppler velocity measurement has an effective way in measuring flow velocity and discharge. However, although the effect of the methods was demonstrated, a little attention has been paid to the flow velocity and the discharge in the anomalous leakage

area of the CFRD. we used it for fixed-depth measurement of the flow velocity in the anomalous area, and obtained the discharge to ensure the consistency of the upstream and downstream leakage, and provide support for the detection results of the flow-field fitting method.

The combination of two approaches formed a novel detection method, and the approaches proposed in this paper are used in CFRD for the first time. It can find out the locations of the leakage area and the discharge quickly, and it can also access to the roughly information of the entire leakage pathways in CFRD. The feasibility of those approaches is verified in case study of the engineering practice.

2. Methods

2.1 Theory of the flow-field fitting method

The flow-field fitting method is a new method to find the leakage locations in CFRD, and a means to detect the leakage distribution characteristics by fitting the seepage field with the current field. In hydraulics, the weak seepage field will be generated around the leakage inlets in CFRD. It is almost impossible to measure directly fluctuations generated by the seepage field with the existing instrument, so the existence of such weak seepage field can only be measured indirectly. The flow of fluid is divided into laminar flow and turbulent flow in porous medium (Bear., 2013). The leakage of the CFRD can be regarded as laminar flow, and the Reynolds number is not more than 1 to 10, the motion of water conforms to Darcy's law (e.g., Reynolds., 1882; Bolève et al.,2007):

$$u = k \cdot H = -k \cdot \nabla\varphi \tag{1}$$

where u denotes the flow velocity, k denotes the permeability coefficient, H denotes hydraulic gradient, and φ denotes the velocity potential, and "−" indicates the direction of the velocity pointing to the potential, and ∇ is the Hamilton operator.

In a Cartesian coordinate system, the three components along the axis are u_x, u_y and u_z. Water is an incompressible fluid that satisfies continuity equations: Flow continuity equation can be written as:

$$\nabla \cdot u = 0 \tag{2}$$

Differential governing equation can be written as:

$$\nabla^2\varphi=0 \tag{3}$$

where ∇^2 denotes the Laplacian.

On the boundary between a fluid and other object, for impermeable surface, water cannot flow through the boundary, that is:

$$\partial\varphi/\partial n=0 \tag{4}$$

and for permeable surface, according to the continuity equation, the normal components of the velocity on the boundary should be equal.

$$\partial\varphi_1/\partial n = \partial\varphi_2/\partial n \tag{5}$$

where n denotes the normal components of the velocity on the boundary, and the subscripts 1 and 2 denote both sides of the boundary.

According to the tutorial (Loke., 2004), for the anomalous point or area, the current vector points to that point or area, and the current density is inversely proportional to the square of the anomalous point or area. For point power supplies, the direction of the current density is to the point source, and the current density is inversely proportional to the square of the distance of the point source. We used the MATLAB software to analyze the simulation of the density curve in current field. It is obvious that the distribution of the density curves is different between Fig.1(a) and Fig.1(b). In the absence of seepage, leakage pathway is similar to a low resistivity object in a homogeneous half-space and current vector points to the inlet of the leakage pathways.

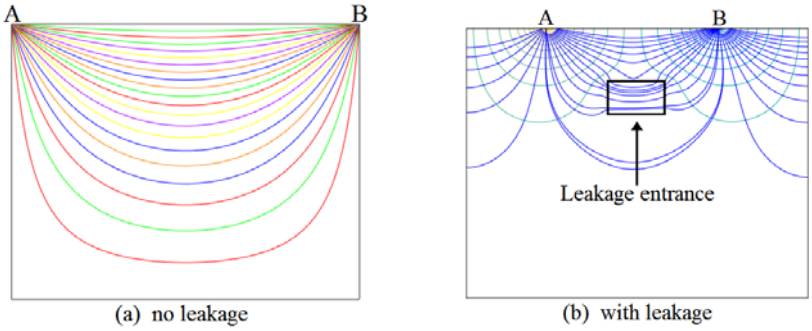

Fig. 1 Comparison of density curve in current field between leakage and no leakage (A and B denote the two current electrodes)

The current field satisfies Ohms law, that is:

$$\mathrm{j} = \sigma \cdot E = -\sigma \cdot \nabla U \tag{6}$$

where j denotes the current density, σ denotes the conductivity, E denotes the electric gradient, and U denotes the electric potential.

Current density continuity equation can be written as:

$$\nabla \cdot j=0 \tag{7}$$

Differential governing equation can be written as:

$$\nabla^2 U=0 \tag{8}$$

On the boundary of the two media, for insulated surface,

$$\partial U/\partial n=0 \tag{9}$$

and for conductive surface, according to the continuity equation, the normal components of the current density on the boundary should be equal.

$$\partial U_1/\partial n = \partial U_2/\partial n \tag{10}$$

where n denotes the normal components of the current density on the boundary, and the subscripts 1 and 2 denote both sides of the boundary.

Table.1 describes the more similarities in mathematical physics between water flow and current. The similarity between seepage field and current field is the theoretical basis for the flow- field fitting method. We convert the velocity potential caused by the leakage pathways into the electric potential. For the current field, the measurement of the potential is simpler and more efficient. Based on this principle, we can use the current field to fit the seepage field, and the measurement of the current field is much easier than the seepage field.

Table.1 Similarities in mathematical physics between seepage field and current field

Seepage field	**Current field**
Velocity potential φ	Electric potential U
Hydraulic gradient H	Electric gradient E
Flow velocity u	Current density j
Permeability coefficient k	Conductivity σ
Normal direction n	Normal direction n
Flow continuity equation $\nabla \cdot u=0$	Current density continuity equation $\nabla \cdot j=0$
Differential governing equation $\nabla^2 \varphi=0$	Differential governing equation $\nabla^2 U=0$
Impermeable surface $\partial\varphi/\partial n=0$	Insulated surface $\partial U/\partial n=0$
Permeable surface $\varphi_{n1}=\varphi_{n2}$	Conductive surface $U_{n1}=U_{n2}$
$\partial\varphi_1/\partial n=\partial\varphi_2/\partial n$	$\partial U_1/\partial n=\partial U_2/\partial n$
Darcy law $u=k\cdot H=-k\cdot\nabla\varphi$	Ohms law $j=\sigma \cdot E=-\sigma \cdot \nabla U$

According to the above method, we can place an aluminum sheet on the upstream and downstream of the CFRD, respectively, and inject a pseudo-random current between two aluminum sheets A and B, and measure the current density distribution in the reservoir area.

2.2 Acoustic Doppler velocity measurement

The acoustic Doppler velocity measurement is a common method used for the measurement of velocity in natural and man-made waterways. The transducer transmits acoustic pulses at a fixed frequency from transducer through the water column and using the Doppler shift of the reflected acoustic energy in each beam computes water velocity profile. Because the water has some suspended particles, a small amount of the sound energy is reflected back (Doppler shift), most of the energy goes forward. Reflected back acoustic wave is received by transducer, and after the reflection signals of different distance can be analyzed (Gordon., 1989). Through tiny differences in the frequency, the velocity of water flow can be calculated used the Doppler shift equation.

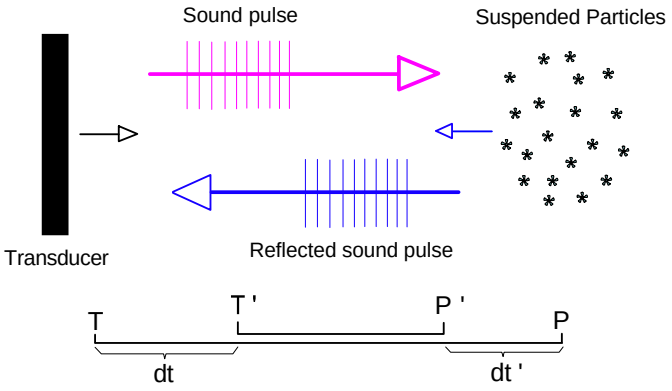

Fig. 2 Layout of Doppler effect principle

Fig.2 illustrates the principle of Doppler shift. T denotes the acoustic source (transmitting transducer), P denotes the observation target (suspended particles), $\mathbf{TT'}$ denotes the motion vector of the acoustic source, and, $\mathbf{PP'}$ denotes the motion vector of the observation target. The vector **TP** from the acoustic source T to the observation target P changes at any time. Supposing the positions of the sound source at time $t = t_0$ and $t = t_0 + dt$ are T and T′ respectively, and the phases are φ and φ' respectively, where the phase increment can be written as:

$$d\varphi = \varphi' - \varphi = 2\pi f_t dt \tag{11}$$

and P reaches P ' ,the phase increment can be written as:

$$d\varphi = 2\pi f_p dt' \tag{12}$$

That is:

$$2\pi f_t dt = 2\pi f_p dt' \tag{13}$$

Rewriting Eq. (13) as:

$$\frac{dt}{dt'} = \frac{f_p}{f_t} \tag{14}$$

The time is $t = t_0 + \frac{\boldsymbol{TP}}{c}$, when the phase ψ propagates from the acoustic source T to the position P of the observation target. The time is $t = t_0 + dt + \frac{\mathbf{T'P'}}{c}$, when the phase $\varphi + d\varphi$ propagates from the acoustic sourceT' to the position P' of the observation target, and the difference between the two is the propagation time from P to P' can be written as:

$$dt' = dt + \frac{\mathbf{T'P'}}{c} - \frac{\boldsymbol{TP}}{c} = dt - \frac{\mathbf{TT'+PP'}}{c} = dt - \frac{v_t dt + v_p dt'}{c} \tag{15}$$

After sorting, we get:

$$\frac{dt}{dt'} = \frac{(c - v_p)}{(c + v_t)} \tag{16}$$

That is:

$$\frac{f_p}{f_t} = \frac{(c - v_p)}{(c + v_t)} \tag{17}$$

Rewriting Eq. (17) as:

$$f_t = \frac{c + v_t}{c - v_p} f_p \tag{18}$$

For acoustic Doppler velocity measurement, the transceiver(observation target) and transducer are inter-related. The transducer is first used as the acoustic source, and the water body is the observation target, so the acoustic wave frequency received by the water body can be written as:

$$f' = \frac{c + v_p}{c - v_t} f_t \tag{19}$$

Then the water body acts as the acoustic source, and the transducer acts as the observation target, so the frequency of the sound wave received by the transducer can be written as:

$$f_p = \frac{c + v_t}{c - v_p} f' \tag{20}$$

Then substituting Eq. (19) into Eq. (20), solving for f_p .

Finally, the Eq. (21) is as follows:

$$f_p = \frac{(c+v_t)(c+v_p)}{(c-v_p)(c-v_t)} f_t \tag{21}$$

When the transmitting transducer measured this time remained stationary during the measurement, then substituting $v_t = 0$ into the Eq. (21):

$$f_p = \frac{(c+v_p)}{(c-v_p)} f_t \tag{22}$$

$$v_p = \frac{f_p - f_t}{f_p + f_t} c \tag{23}$$

Defining $f_d = f_p - f_t$, Eq. (23) can be rewritten as:

$$v_p = \frac{f_d}{2f_t} c \tag{24}$$

where v_p denotes the radial velocity of water relative to the transducer, f_d denotes the Doppler shift, f_t denotes the frequency of the transmitting transducer, and c denotes the velocity of sound in the water.

We used the acoustic Doppler current profiler (ADCP) for depth measurement of the flow velocity in the center of the abnormal area based on Doppler effect. The data collected by ADCP is substituted into equation 24, and obtained the flow velocity.

3. Case study

3.1 Study area

Project area is located at Luquan County, Yunnan Province, China. The upstream is the Lujichang hydropower station, and the downstream is the Baihetan hydropower station on the main stream of the Jinsha River. Project area is 150km away from Luquan County and 220km away from Kunming Highway (Fig.3). The project area is concrete face rockfill dam, and the highest height and length of the dam are 100m and 430m, respectively. Fig.4 shows typical profile of CFRD. The total reservoir capacity is about 185 million m^3. After the reservoir was impounded, leakage was found around the right abutment and observed in the flow measurement weir of the downstream, as shown in Fig.3. The color of the leakage water was turbid, and after days later became clear. The discharge was stable in the range of 120L/s~140L/s. The aim of this case study is to investigate the leakage areas

in the reservoir area of the upstream, estimate the discharge in the leakage areas, ensure that there is no other leakage around the dam and provide technical supports and solutions about the layout of grouting holes to prevent or repair leakage.

Fig. 3 Photographs showing geographical location of the studied dam and the leakage area

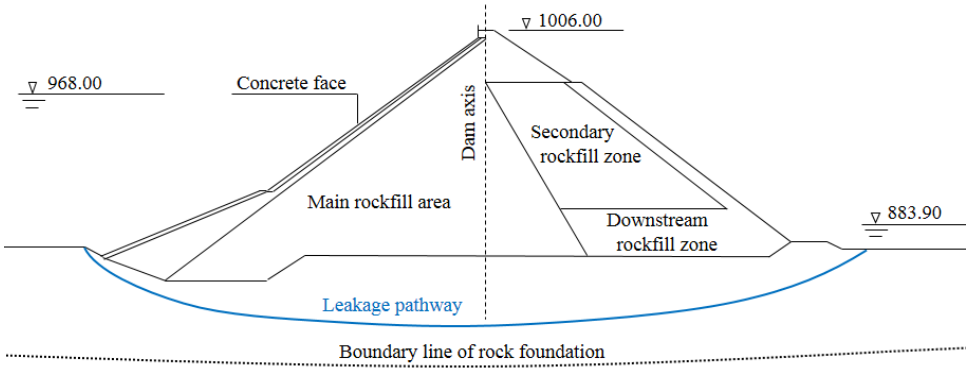

Fig. 4 Typical profile of CFRD (unit of water level and elevation: m). Normal water level is 968.00m, downstream flow measurement weir level is 883.90m, crest elevation is 1006.00m.

3.2 Numerical simulation about leakage of the CFRD

The goal of this section is to study whether it is reasonable to fit the seepage field with the current field in the CFRD. The main hydraulic structures of the CFRD were numerically simulated according to the original layout of the CFRD body. A finite element model was established to analyze the simulation of the seepage field. In hydraulics, the weak seepage field will be generated around the leakage inlets in dams. The existence of such weak seepage field can be observed directly based on ANSYS software. We use the commercial software ANSYS Fluent 2020 R2, which is a partial differential equation solver.

Three-dimensional size of CFRD is built as (Fig.5a): a dam's length is 85mm, width is 60mm, height is 50mm, and the dam model is symmetric about the Y axis. The reservoir water is 25mm in depth, and its resistivity is 50Ω·m. Top face of the reservoir water is 50mm in length, 52mm in width, and bottom face is 50mm in length, 40mm in width. The leakage pathway is a cylinder with a diameter of 1mm and a length of 15mm, and the inlet in the upstream face of dam, is (0mm,50mm,15mm), and the outlet in the downstream of dam, is (0mm,65mm,15mm). The resistivity of the leakage pathway is 20Ω·m.

Unstructured elements are used to perform the finite element mesh. The finite element mesh of the water body and leakage pathway are represented in Fig.5b. Volume statistics is as follows: minimum volume is $5.57\times10^{-5}mm^3$, maximum volume is $2.05mm^3$, and total volume is $5.96\times10^{4}mm^3$. The direction of gravity is the Z direction, and the value is -9.81m/s^2. Material is water-liquid, and the value of the viscous resistance and the inertial resistance is the default. The porosity of leakage pathway is 0.2. For the problem of the dam leakage, atmospheric pressure boundary condition was applied to the boundaries. Coupled solution method was used to steady-state condition. After setting the monitoring parameters, just run the calculation. The velocity distribution at or near the inlets of leakage is obtained by numerical simulation.

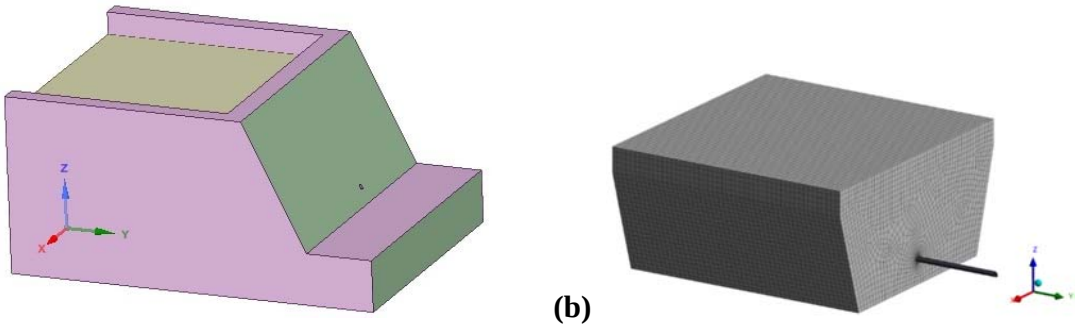

(a) **(b)**

Fig.5 Three-dimensional model of CFRD and reservoir. (a) The model of dam. (b) The finite element mesh of reservoir water and leakage pathway

As previously described, Darcy's law has its limits, the effects of the Reynolds number need be taken into account. When the Reynolds number is not more than 1 to 10, the motion of water conforms to Darcy's law. Fig.6 shows the range of Reynolds number, the maximum is nearly 5, therefore, it is reasonable to use current field method to fit the seepage field.

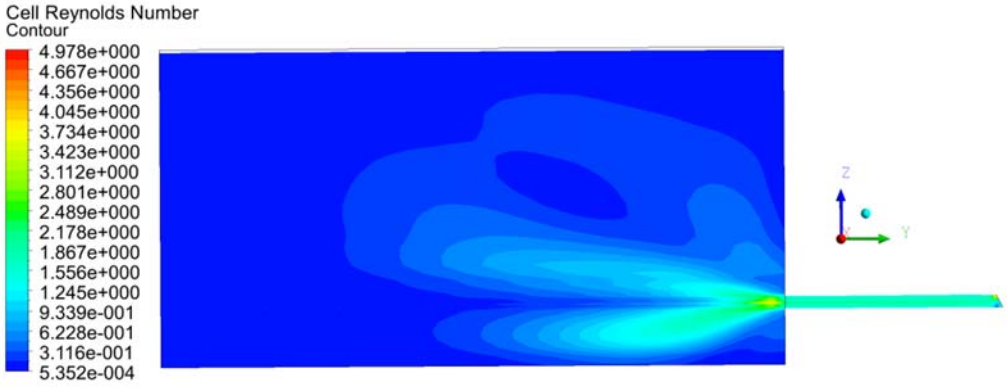

Fig.6 Reynolds number diagram in YZ plane

Fig.7 shows three slices velocity diagrams at Y=15mm, 35mm, 49mm on the ZX plane, respectively. It is not obvious in linear form, so the velocity contour color is shown in logarithmic form. The distribution of the flow velocity can be observed, and it is obvious that: the closer to the leakage inlet, the greater the velocity value is. Fig.8 shows that in the absence of seepage, the seepage field converts to anomalous seepage field caused by leakage appear. The important feature of the abnormal seepage field is that the water flow velocity vector points to the leakage inlets.

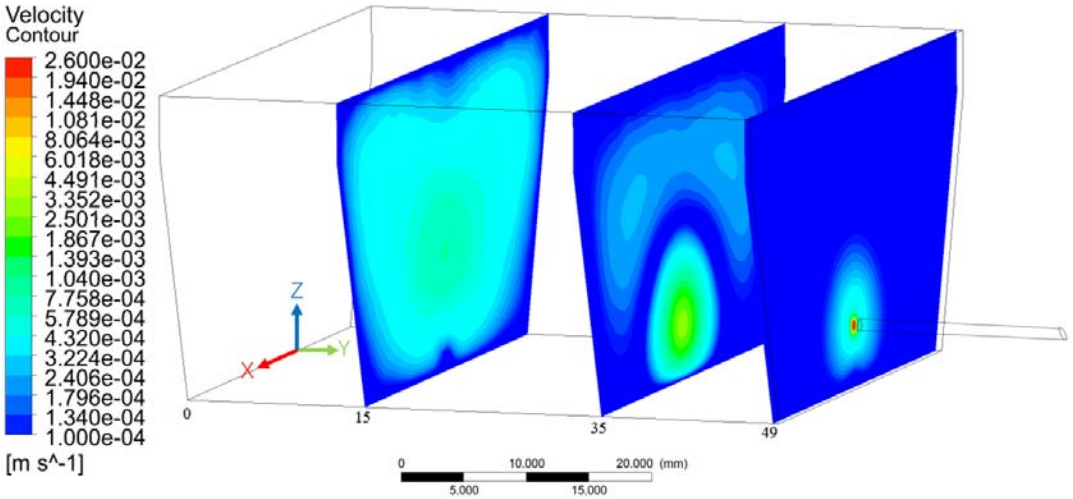

Fig.7 Slice velocity diagram in ZX plane (Y=15mm, 35mm, 49mm)

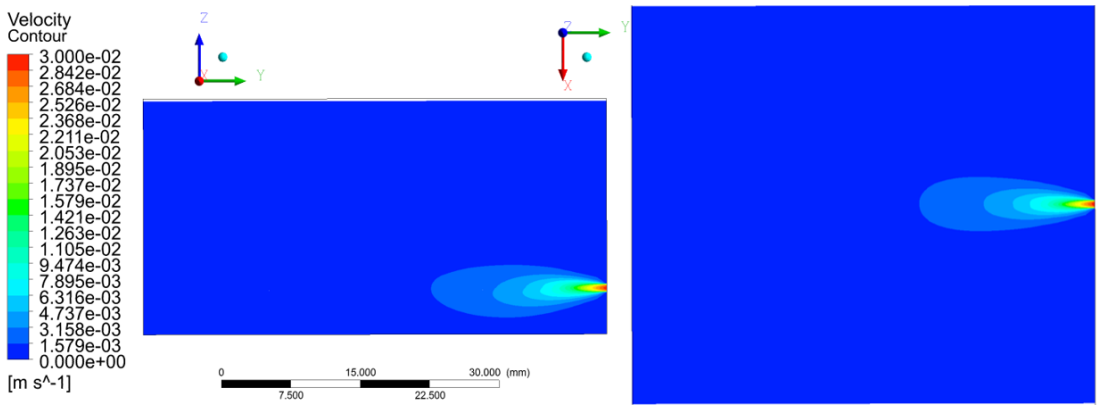

(a) (b)

Fig.8 Slice velocity diagram. (a) is in YZ plane (X=0mm); (b) is in XY plane (Z=15mm)

Fig.9(a) shows the location of three monitoring lines. Fig.9(b), (c) and (d) show a comparison between flow velocity and different axes. In Fig.9(b), the red monitoring line of X=0mm, Z=15mm passes from Y=0mm to Y=60mm (leakage inlet is X=0mm,Y=50mm, Z=15mm), shows that with the closer to inlet, the value of flow velocity is getting bigger, and velocity is biggest in the inlet. The distribution of blue monitoring line of Y=49mm, Z=15mm appears symmetrical in X=0mm, just as Fig.9c as shown, and velocity emerge extremums at X=0mm. In Fig.9d, the green monitoring line of X=0mm, Y=49mm passes from Z=10mm to Z=35mm (leakage inlet is X=0mm,Y=50mm, Z=15mm), the trend of the green monitoring line is similar to Fig.9(c), but the maximum value is close to twice the blue monitoring line.

By contrasting and analyzing three survey lines in Fig.9, the value of velocity in Y-component and Z-component is nearly twice the X-component. Furthermore, the change of velocity around the leakage inlet is more obvious in the Z-component comparing to the Y-component. The result identifies the main component of the velocity Z responsible for the flow velocity signature. Therefore, the leakage location and probable inlets can easily obtain through the Z-component.

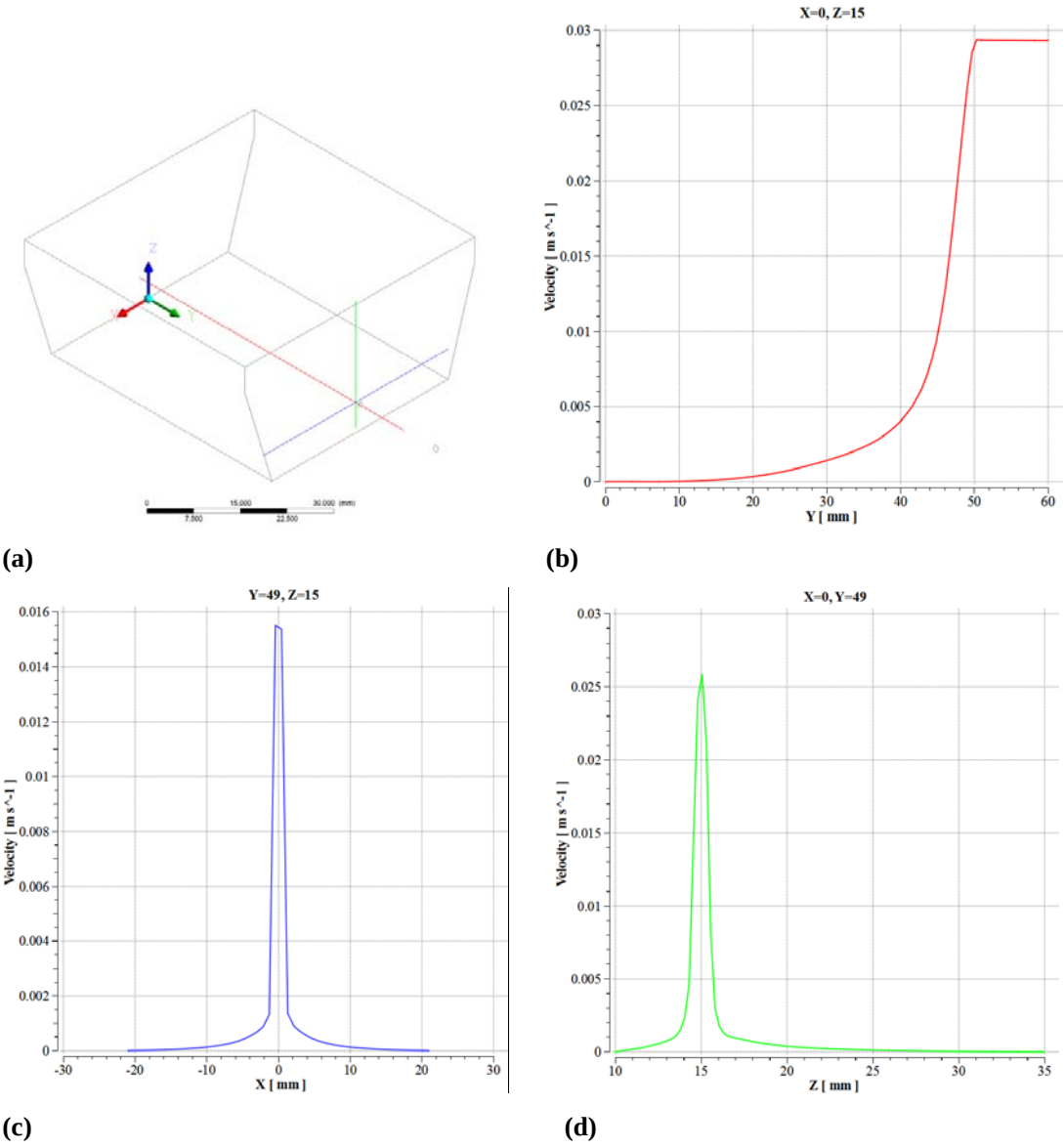

(a) **(b)**

(c) **(d)**

Fig.9 Distribution of flow velocity in three monitoring lines

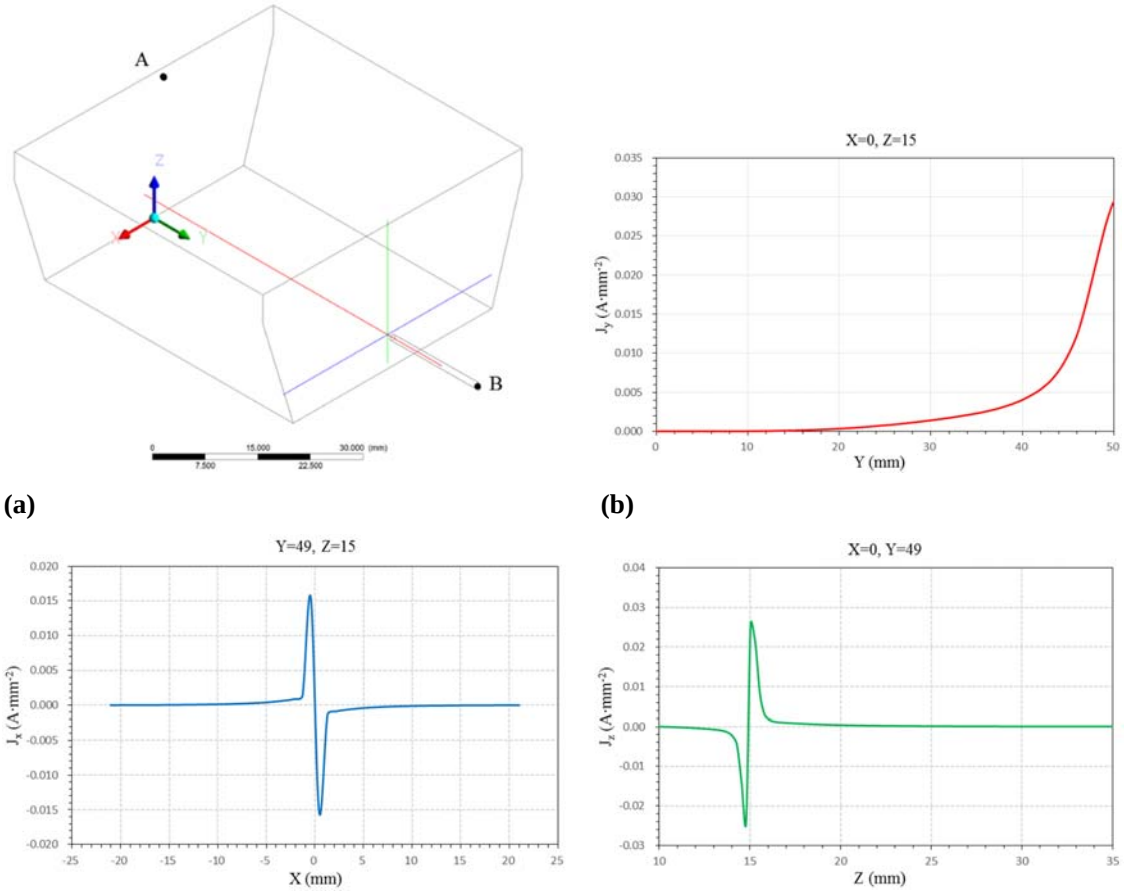

(a) **(b)**

(c) **(d)**

Fig.10 Distribution of current density in three monitoring lines

To get the distribution of the current density, the current is applied in the faraway upstream section, and the injection electric current is set as 2A in the simulation between two electrodes A and B separated by a distance of 60 mm (Fig.10a). The distribution of the current density at or near the inlets of leakage is obtained by numerical simulation. Fig.10(b), (c) and (d) show a comparison between current density and different axes (X-component, Y-component, Z-component). The distribution of three monitoring lines is the same as the distribution of the three lines in Fig.9. Fig.10(b) shows that with the closer to inlet, the value of current density is getting bigger. Fig.10(c) and Fig.10d show that the current density at the inlet of the leakage has a positive maximum and a negative minimum. By contrasting and analyzing the slope of the current density of the three survey lines at the inlet of the leakage, the rate of change of the X and Z components of the current density is larger than Y-component, moreover, the extremums at Z-component is nearly twice the

X-component. The result identifies the main component of the current density J_Z responsible for the current signature. Therefore, the leakage location and probable inlets can also easily and quickly obtain through the Z-component of the current density.

3.3 Leakage detection based on the flow-field fitting method

The field work took approximately one day to complete. The detection method is shown in Fig. 11. To best characterize the leakage pathways, the energizing aluminum sheets A and B must be strategically placed upstream and downstream. The upstream aluminum sheet is far away from the water outlet to ensure the current field of measurement area not affected by each other. We regard the distance between aluminum sheet A and aluminum sheet B to be as far as possible, and no less than five times the length of the overall detecting area, just as shown in Fig.11. We proposed to use aluminum sheets instead of electrodes. Compared with electrodes, aluminum sheets can better generate and receive current signals in the long-distance transmission. According to the above-mentioned physical facts and the result of numerical simulation, the probe 's Z component was used to detect changes in current density in the reservoir area.

An DC electric current with a pseudo-random signal was applied to the paired (A, B) aluminum sheets. The electric current flowing between the aluminum sheets (A, B) generates a current field. We used the transmitter to supply pseudorandom signal to the two aluminum sheets linked to cable. Lastly, we put the probe linked to the receiver into the water, and by controlling the travel route of the boat, we use music monitoring and meter display to find the seepage area, and we use a differential GPS for positioning at a certain distance. The detected current density value is converted to voltage value, which is reflected in the way of sound. The greater the voltage, the louder the sound, and results indicated the possible presence of leakage.

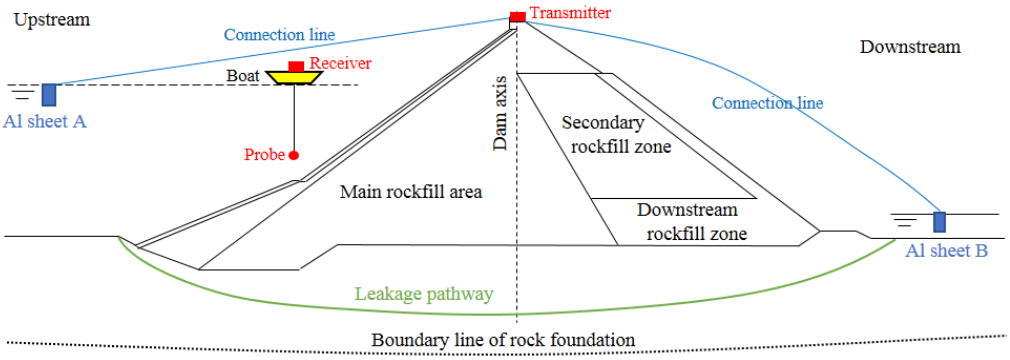

Fig. 11 Simple diagram showing the arrangement of the leakage survey and the basic principle of the method to measure the leakage area

We can determine the leakage locations by analyzing the distribution of the voltage section in the horizontal plane. Measured values have varied degrees of response at the site of leakage. The background values of potential difference are about 0-30 mV (Fig.12), therefore we took the values between 0-30 mV as the normal areas, and regard values higher than it as anomalous areas. Thus, by the analysis of the detection data of each survey line and measuring point (with a differential GPS), three anomalous areas were found on the right bank of the reservoir area (the detected locations were significantly higher than the background value of the nearby area).

The chromatogram of the flow-field fitting method was shown in Fig.12. The three anomalous areas were presumed to be leakage inlets, and the others indicated no leakage. Among them, the area of No.1 anomalous area was about 2000m^2, the area of No.2 was about 80m^2, and No.3 was about 120m^2.

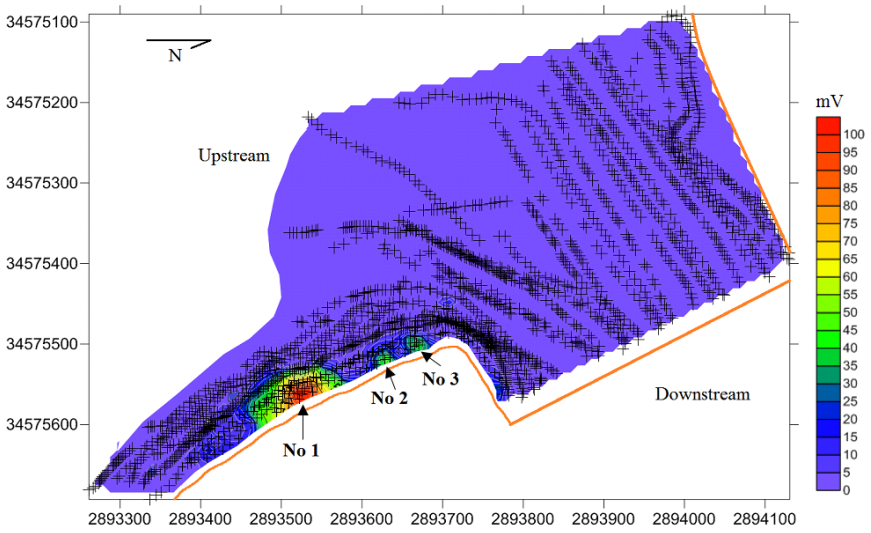

Fig. 12 Chromatogram of potential difference about reservoir area ("×" denotes a differential GPS measuring point)

3.4 Velocity analysis based on the acoustic doppler effect

The acoustic doppler velocity profiler (ADCP) has been extensively used for velocity analysis in natural rivers and streams. ADCP was used to measure the velocity near the center of the No.1 to No.3 anomalous area in the reservoir area, and the results of radial velocity distribution varying with depth were obtained. We used it for fixed-depth measurement of the flow velocity at the center of the anomalous area (see Fig.13).

According to the actual depth of the leakage area in the dam, 600kHz working frequency of the transducer was used. Working technical specifications of the acoustic Doppler velocity profiler in China is shown in Table.2.

Table 2 Working parameter list of the ADCP

Frequency of operation /kHz	38	75	150	300	600	1200
Initiative measured depth /m	16.0	8.0	4.0	2.0	1.0	0.5
Maximal measured depth /m	700	350	180	100	50	20

The transducer transmits acoustic pulses at a fixed frequency from transducer through the water column and using the Doppler shift of the reflected acoustic energy in each beam computes water velocity profile. the velocity can be calculated used the Doppler shift equation 24.

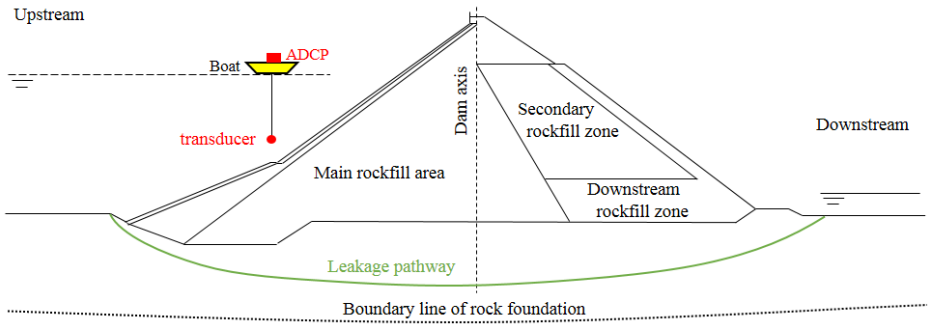

Fig. 13 Simple diagram showing the arrangement of the flow velocity measurement in leakage area

According to the curves of depth-flow velocity (Fig.14), and there was a water flow of 0.012~0.093m/s in the No.1 anomalous area, there was a water flow with a velocity of 0.021~0.072m/s in the No.2 anomalous area, and a water flow with a velocity of

411 0.014~0.073m/s in the No.3 anomalous area. See Fig.14 for details. Taking into account
412 the wind and waves on the day of the measurement, the measured flow velocity is within
413 the depth range of 5m-30m. The average flow velocity of the three abnormal areas were
414 0.064m/s, 0.052m/s, and 0.054m/s, respectively. In addition, the estimated area of No.1
415 anomalous area was 2000m^2, the area of No.2 was 80m^2, and No.3 was 120m^2, respectively.
416 We used the index velocity method (e.g., Le Coz et al., 2008; Levesque et al., 2012)
417 to predict the discharge from the ADCP, and based on previous engineering experience
418 (e.g., Nord et al., 2014; Kästner et al., 2018), the discharge in the No. 1 to No. 3 abnormal
419 areas was estimated to be 95 L/s, 15 L/s and 20 L/s, respectively. The calculated total
420 discharge (130L/s) was in agreement with the flow measurement weir of the downstream
421 (120L/s~140L/s).

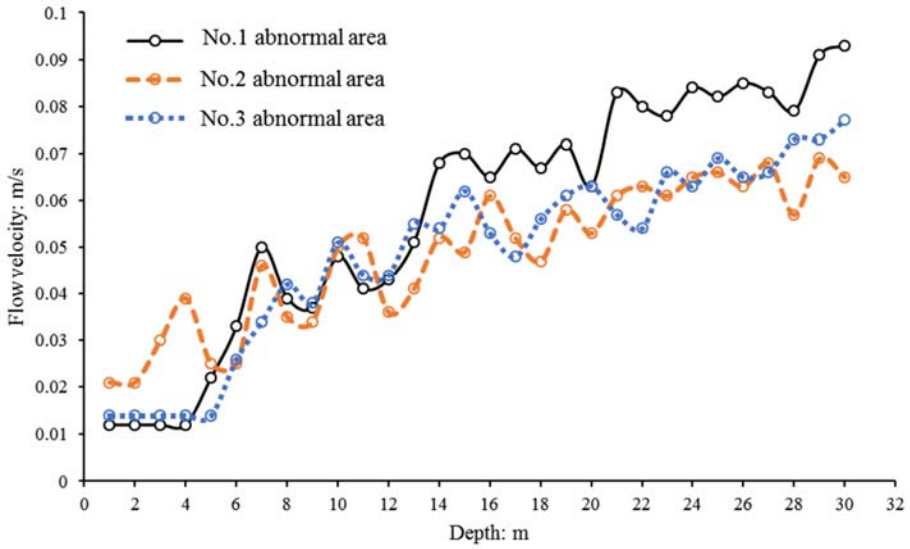

422
423 **Fig.14** Curves of Depth-Flow velocity

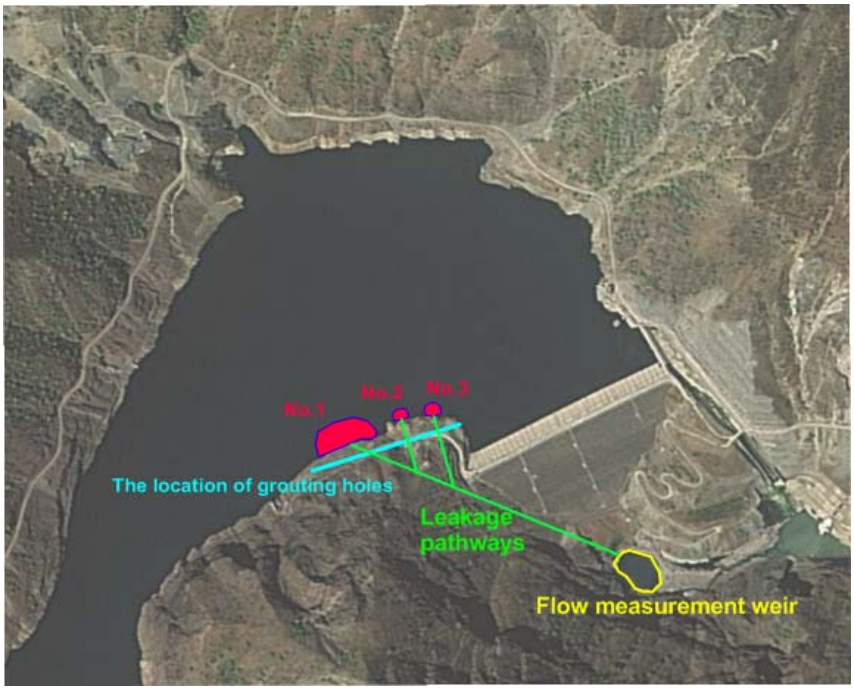

Fig. 15 Detection results in investigation area

3.5 Final result

The numerical simulation results showed that the seepage field can be fitted with the current field, and the leakage location and probable inlets can easily and quickly obtain through the Z-component of the current field. According to the actual situation in the study area, and from the profile of results provided by the flow-field fitting method, it is capable to identify the leakage locations and the scale of leakage area. In addition, acoustic Doppler velocity measurement determines the flow velocity in the upstream, and roughly calculates the discharge, and it is basically the same as the discharge measured in the measuring weir of the downstream. As shown in Fig.12, three anomalous areas were detected, and comparing the calculated leakage with the flow measurement weir of the downstream (see Fig.14), it shows that there are no other leakage areas around the dam. Based on the on-site investigation results (see Fig.15), there are roughly three leakage pathways and no other leakage pathways in the reservoir area. This type of information can be used to take effective decisions concerning how to further monitor and remediate ground water bypassing upstream into the flow measurement weir of the downstream.

4. Discussions

As shown in the previous sections, the flow-field fitting method and acoustic Doppler velocity measurement can be used to determine leakage inlets and conductive pathways, which can be interpreted, under specific circumstances, to preferential leakage pathways of ground water. These leakage inlets can be hardly detected using other techniques. The correspondence between electrical and hydraulic flow is only apparent and works only in some cases. In addition, electrical resistivity imaging is limited by its lack of resolution and the inability to place electrodes on the concrete surface. Induced polarization is sensitive to permeability but suffer from the same limitations than electrical resistivity tomography regarding its resolution. The self-potential is sensitive to the mineralization of the pore water and highly mineralized ground water implies low self-potential signals.

Another point worth to be discussed is the fact that the flow-field fitting method is widely used in china, but it is rarely mentioned abroad. In addition, one may wonder about the validity of the fitting method used in this paper while we use it to detect leakage inlets in the CFRD. In this paper, we have neglected the case where the Reynolds number is greater than 10. We will need however to check in future publications if this assumption is always valid, especially for the current field distribution in the non-Darcy. The use of three component current density sensors should be considered in future research, and it should be able to improve the accuracy of detection.

Our methods can be used to access to the roughly information of the entire leakage pathways, and this technique works well when we know where the leakage pathways start or end, and it has the advantage of taking measurements in the water, without requiring contact with the surface of the CFRD. This is an interesting research topic in itself.

5. Conclusions

The flow-field fitting method and the acoustic Doppler velocity measurement appear as a novel method for leakage investigation of CFRD compared with conventional geophysical methods. In our case study, the two methods showed an enormous potential for large-scale leakage detection of CFRD. Three leakage pathways have been found, and there is no leakage around the dam. It is the key point of dam foundation reinforcement

project to determine the best position of grouting borehole according to the results. By optimizing the layout of grouting holes through geophysical investigation, the number of drilling holes can be reduced and the engineering cost can be saved. The flow-field fitting method can also be combined with other geophysical methods to detect leakage pathways in CFRD. When the CFRD is at low water level, appropriate anti-seepage materials and seepage grouting can be used to repair or block the leakage area.

Acknowledgments

The authors appreciate the supports provided by the National Natural Science Foundation of China (41374116 and 41674113). The authors also acknowledge Yellow River Institute of Hydraulic Research for providing the field data.

Data Availability Statement: the data supporting the conclusions can be obtained by: https://doi.org/10.6084/m9.figshare.14703021

Reference

Abdulsamad, F., Ahmed, A., Coperey, A., Karaoulis, M., Nicaise, S. & Peyras, L. 2019. Induced polarization tomography applied to the detection and the monitoring of leaks in embankments. *Engineering Geology, 254*, doi: 10.1016/j.enggeo.2019.04.001.

Ahmed, A., Bolève, A., Steck, B., Vergniault, C., Courivaud, J.R., Jougnot, D. & Abbas, M. 2020. Determination of the permeability of seepage flow paths in dams from self-potential measurements. *Engineering Geology, 268*, 105514,doi:10.1016/j.enggeo.2020.105514.

Ahmed, A., Steck, B., Vergniault, C., Jardani, A. & Vinceslas, G. 2019. Self-potential signals associated with localized leaks in embankment dams and dikes. *Engineering Geology, **253***, doi: 10.1016/j.enggeo.2019.03.019.

Antoine, R., Fauchard, C., Fargier, Y. & Durand, E. 2015. Detection of Leakage Areas in an Earth Embankment from GPR Measurements and Permeability Logging. *International Journal of Geophysics, 2015, 9*, doi: 10.1155/2015/610172.

Bear, J., 2013. Dynamics of fluids in porous media, First edition. Dover Publications, New York.

Bahreinimotlagh, M., Kawanisi, K., Danial, M., Al Sawaf, M.B. & Kagami, J. 2016. Application of shallow-water acoustic tomography to measure flow direction and river discharge. *Flow Measurement and Instrumentation, 51*, 30-39, doi: 10.1016/j.flowmeasinst.2016.08.010.

Battaglia, D., Birindelli, F., Rinaldi, M., Vettraino, E., Bezzi, A., 2016. Fluorescent tracer tests for detection of dam leakages: the case of the Bumbuna dam-Sierra Leone.*Eng. Geol. 205*, 30–39. dio:10.1016/j.enggeo.2016.02.010.

Boldt, J. & Oberg, K. 2015. Validation of Streamflow Measurements Made with M9 and RiverRay Acoustic Doppler Current Profilers. *Journal of Hydraulic Engineering, 142*, 04015054, doi: 10.1061/(ASCE)HY.1943-7900.0001087.

Bolève, A., Crespy, A., Revil, A., Janod, F., Mattiuzzo, J. L., 2007. Streaming potentials of granular media: Influence of the Dukhin and Reynolds numbers. *Journal of Geophysical Research, 112(B8)*.

Bolève, A., Vandemeulebrouck, J. & Grangeon, J. 2012. Dyke leakage localization and hydraulic permeability estimation through self-potential and hydro-acoustic measurements: Self-potential 'abacus' diagram for hydraulic permeability estimation and uncertainty computation. *Journal of Applied Geophysics, 86*, 17-28, doi: 10.1016/j.jappgeo.2012.07.007.

Cho, I.-K., Yeom, J.-Y., 2007. Crossline resistivity tomography for the delineation of anomalous seepage pathways in an embankment dam. *Geophysics 72*, G31–G38.

Desir, G. & Gutierrez, M. 2003. Causes of the catastrophic failure of an earth dam built on gypsiferous alluvium and dispersive clays (Altorricón, Huesca Province, NE Spain). *Environmental Geology, 43*, 842-851, doi: 10.1007/s00254-002-0700-2.

Fargier, Y., Lopes, S., Fauchard, C., François, D. & Cote, P. 2014. DC-Electrical Resistivity Imaging for embankment dike investigation: A 3D extended normalisation approach. *Journal of Applied Geophysics, 103*, doi: 10.1016/j.jappgeo.2014.02.007.

Ferdos, F., Dargahi, B. & Solari, L. 2018. Mechanism of Suffusion Erosion Phenomenon In Porous Media.

Gordon, R. L. (1989). Acoustic measurement of river discharge. *Journal of Hydraulic Engineering, 115(7)*, 925–936.

Gunawan, B., Sterling, M. & Knight, D. 2010. Using an Acoustic Doppler Current Profiler in a Small River. *Water and Environment Journal, **24***, 147-158, doi: 10.1111/j.1747-6593.2009.00170.x.

He., J. 1999. Detection Technology of Leakage Pipeline "Flow Field Method". *Copper Engineering (Chinese Journal), 01*, 5-8.

Howard, A. & McLane Iii, C. 1988. Erosion of cohesionless sediment by groundwater seepage. *Water Resources Research - WATER RESOUR RES, **24***, 1659-1674, doi: 10.1029/WR024i010p01659.

Jardani A, Dupont JP, Revil A (2006a) Self-potential signals associated with preferential ground water flow pathways in sinkholes. *J Geophys Res 111:B09204*. doi:10.1029/2005JB004231

Jardani, A., Revil, A., Bol`eve, A. & Dupont, J.P., 2008. 3D inversion of self-potential data used to constrain the pattern of ground water flow in geothermal fields, *Journal of Geophysical Research, 113*, B09204, doi:10.1029/2007JB005302.

Kästner, K., Hoitink, A.J.F., Torfs, P.J.J.F., Vermeulen, B., Ningsih, N.S. & Pramulya, M. 2018.

Prerequisites for Accurate Monitoring of River Discharge Based on Fixed-Location Velocity Measurements. *Water resources research, 54*, 1058-1076, doi: 10.1002/2017wr020990.

Klema, M., Pirzado, A., Venayagamoorthy, S. & Gates, T. 2020. Analysis of acoustic Doppler current profiler mean velocity measurements in shallow flows. *Flow Measurement and Instrumentation, **74***, 101755, doi: 10.1016/j.flowmeasinst.2020.101755.

Loke, M.H., 2004. Tutorial: 2-D and 3-D Electrical Imaging Surveys.

Le Coz, J., Pierrefeu, G., & Paquier, A. (2008). Evaluation of river discharges monitored by a fixed side looking Doppler profiler. *Water Resources Research, 44*, W00D09. https://doi.org/10.1029/2008WR006967

Le Menn, Marc & Morvan, Steffen. (2020). Velocity Calibration of Doppler Current Profiler Transducers. *Journal of Marine Science and Engineering. 8*. 847. 10.3390/jmse8110847.

Levesque, V. A., & Oberg, K. A. (2012). Computing discharge using the index velocity method (Techniques and Methods 3, Report no. A-23,148 pp.). Reston, VA: U.S. *Geological Survey*.

Martínez-Moreno, F., Delgado-Ramos, F., Galindo-Zaldívar, J., Martín-Rosales, W., Manuel, L.-C. & González-Castillo, L. 2018. Identification of leakage and potential areas for internal erosion combining ERT and IP techniques at the Negratín Dam left abutment (Granada, southern Spain). *Engineering Geology, 240*, doi: 10.1016/j.enggeo.2018.04.012.

Meng, Y., Fang, Y., Wan, M., Su, Q., Tian, B. & Tong, F. 2018. Research of concrete dam leakage detection based on anomaly current field of reservoir water. *Journal of Applied Geophysics, 160*, doi: 10.1016/j.jappgeo.2018.11.016.

Münchow, A., Coughran, C., Hendershott, M. & Winant, C. 1995. Performance and Calibration of an Acoustic Doppler Current Profiler Towed below the Surface. *Journal of Atmospheric and Oceanic Technology - J ATMOS OCEAN TECHNOL, **12***, doi: 10.1175/1520-0426(1995)012 <0435:PACOAA>2.0.CO;2.

Nord, G., Gallart, F., Gratiot, N., Soler, M., Reid, I., Vachtman, D., Latron, J., Martín-Vide, J.P. & Laronne, J.B. 2014. Applicability of acoustic Doppler devices for flow velocity measurements and discharge estimation in flows with sediment transport. *Journal of hydrology (Amsterdam), 509*, 504-518, doi: 10.1016/j.jhydrol.2013.11.020.

Oberg, K., Mueller, D. & Asce, M. 2007. Validation of Streamflow Measurements Made with Acoustic Doppler Current Profilers. *Journal of Hydraulic Engineering-asce - J HYDRAUL ENG-ASCE, 133*, doi: 10.1061/(ASCE)0733-9429(2007)133:12(1421).

Prinzio, M.D., Bittelli, M., Castellarin, A., Pisa, P.R., 2010. Application of GPR to themonitoring of river embankment. *J. Appl. Geophys. 71*, 53–61.

Qianwei, D., Lin, F., Wang, X., Feng, D.-S. & Bayless, R. 2017. Detection of concrete dam leakage using an integrated geophysical technique based on flow-field fitting method. *Journal of Applied Geophysics, 140,* doi: 10.1016/j.jappgeo.2017.03.013.

571 Rizzo E, Suski B, Revil A, Straface S, Troisi S (2004) Self-potential signals associated with pumping-
572 tests experiments. *J Geophys Res 109:B10203*. doi:10.1029/2004JB003049
573 Revil, A., Binley, A., Mejus, L. & Kessouri, P., 2015. Predicting permeability from the characteristic
574 relaxation time and intrinsic formation factor of complex conductivity spectra, *Water Resour. Res., 51*,doi:10.1002/2015WR017074.
575
576 Revil,A.,Karaoulis,M.,Johnson,T.&Kemna,A.,2012.Review:some low-frequency electrical methods for
577 subsurface characterization and monitoring in hydrogeology, *Hydrogeol. J., 20(4),* 617–658.
578 Reynolds, O. 1882. An Experimental Investigation of the Circumstances Which Determine Whether
579 the Motion of Water Shall Be Direct or Sinuous, and of the Law of Resistance in Parallel
580 Channels.Phil.Trans. *R. Soc., 935*, doi: 10.1098/rstl.1883.0029.
581 Sjodahl, P., Dahlin, T., Johansson, S., Loke, M.H., 2008. Resistivity monitoring for leakage and internal
582 erosion detection at Hallby embankment dam. *J. Appl. Geophys. 65(3–4)*, 155–164.
583 Unal, B., Eren, M. & Yalcin, M. 2007. Investigation of leakage at Ataturk Dam and hydroelectric
584 power plant by means of hydrometric measurements. *Engineering Geology, 93*, 45-63,
585 doi: 10.1016/j.enggeo.2007.02.006.
586 Xu, X., Zeng, Q., Li, D., Wu, J., Wu, X. & Shen, J. 2010. GPR detection of several common
587 subsurface voids inside dikes and dams. *Engineering Geology - ENG GEOL, 111*,
588 31-42, doi:10.1016/j.enggeo.2009.12.001.